in vivo *31*: 779-791 (2017)
doi:10.21873/invivo.11131

Tissue-directed Implantation Using Ultrasound Visualization for Development of Biologically Relevant Metastatic Tumor Xenografts

RAELENE A. VAN NOORD[1], TINA THOMAS[1], MELANIE KROOK[2], SAHITI CHUKKAPALLI[1], MARK J. HOENERHOFF[3], JONATHAN R. DILLMAN[4], ELIZABETH R. LAWLOR[2,5], VALERIE P. OPIPARI[5] and ERIKA A. NEWMAN[1]

Departments of [1]Surgery, [2]Pathology, [4]Radiology and [5]Pediatrics, C.S Mott Children's and Women's Hospital, Mott Solid Tumor Oncology Program, The University of Michigan Medical School, Ann Arbor, MI, U.S.A.; [3]Unit for Laboratory Animal Medicine, The University of Michigan Medical School, Ann Arbor, MI, U.S.A.

Abstract. *Background: Advances in cancer therapeutics depend on reliable in vivo model systems. To develop biologically relevant xenografts, ultrasound was utilized for tissue-directed implantation of neuroblastoma (NB) cell line and patient-derived tumors in the adrenal gland, and for renal subcapsular engraftment of Ewing's sarcoma (ES). Materials and Methods: NB xenografts were established by direct adrenal injection of luciferase-transfected NB cell lines (IMR32, SH-SY5Y, SK-N-BE2) or NB patient-derived tumor cells (UMNBL001, UMNBL002). ES xenografts were established by renal subcapsular injection of TC32, A673, CHLA-25, or A4573 cells. Progression was monitored by in vivo imaging. Results: Tumors progressed to local disease with metastasis evident by 5 weeks. Metastatic sites included cortical bone, lung, liver, and lymph nodes. Xenografted tumors retained immunochemical features of the original cancer. Conclusion: Human NB adrenal xenografts, including two patient-derived orthotopic, and ES renal subcapsular xenografts were established by ultrasound without open surgery. Tissue-directed implantation is an effective technique for developing metastatic preclinical models.*

In order to better understand tumor biology and to examine new therapeutic approaches, cancer researchers often utilize animal xenograft models for preclinical drug screening. Compared to cell-based *in vitro* studies, animal models more accurately replicate three-dimensional tumors and minimize utilization of artificial biological factors in culture. Early models relied on flank injection of cancer cells with subcutaneous heterotopic tumor engraftment, allowing for rapid assessment of growth and response to therapeutics. While these models have been broadly utilized in drug discovery because of their relatively low costs and ease of use, they are often inconsistent in later stages of clinical development and rarely demonstrate important disease characteristics such as the capacity to metastasize. The etiology of this discrepancy is multifactorial, but likely largely due to complexities in the interactions between tumors and the host microenvironment (1). In contrast, orthotopic cancer models have been found to closely replicate native tumor histopathology and enhance metastatic potential (2). It has now been established that engraftment of human cancer cells into the appropriate anatomical sites maintains original biological features of cancer growth with metastasis, and provides more accurate models than subcutaneous xenografts for drug discovery (3, 4). Orthotopic models have been further enhanced by implantation of fresh patient-derived cells, rather than established cell line-based xenografts. There is strong evidence that cell lines maintained in serum-containing growth media harbor greater genetic divergence from the primary tumor than direct xenografts, which may have functional implications in preclinical work (5). This provides evidence that development of reliable patient-derived orthotopic xenografts is an important improvement over standard models for investigation of new therapies and diagnostic imaging modalities.

There is a particularly strong need to develop improved models for preclinical studies of neuroblastoma (NB), the

Correspondence to: Erika A. Newman, MD, FACS, FAAP, C.S. Mott Children's and Women's Hospital, 1040 E. Hospital Dr., Ann Arbor, MI 48109, U.S.A. Tel: +1 7347646482, Fax: +1 7342328667, e-mail: eanewman@med.umich.edu

Key Words: Ewing's sarcoma, neuroblastoma, orthotopic, preclinical model, ultrasound, xenograft.

most common solid tumor type in infants. It is estimated that NB accounts for approximately 5% of pediatric cancer diagnosis and disproportionately constitutes up to 10% of cancer mortality in children (6). The clinical course and overall prognosis is biologically diverse, ranging from spontaneous regression in neonates to resistant disseminated disease in older children. Although steady improvements have been made in survival of children with lower stage disease, the survival rates for patients with high-risk NB is often <40% despite aggressive surgery and myeloablative chemotherapy (7). For these reasons, it is critical that preclinical model systems are optimized to recapitulate the complexities of original tumors for therapeutic development.

Compared to subcutaneous models, orthotopic NB models have been shown to retain major characteristics of the primary tumor and develop metastases to distant organs (8). Moreover, NB patient-derived xenografts retain genetic and morphological characteristics of the primary tumor (9). NB arises from the adrenal glands and the paravertebral sympathetic chain, therefore orthotopic implantation requires trans-abdominal or retroperitoneal access, typically *via* open surgery. This is a time-consuming skill that is technically challenging, with complicated animal recovery periods. In order to address the challenges of microsurgery, several reports have utilized high-resolution ultrasound for guided orthotopic implantation of tumor cells (10, 11). This approach allows percutaneous access to murine abdominal viscera and may provide efficient and safe development of relevant cancer xenografts. Ultrasound guidance provides a minimally invasive option that addresses the existing limitations of traditional orthotopic models (10).

We established three human NB cell line (SH-SY5Y, SK-N-BE2, IMR32) and two patient-derived (UMNBL001, UMNBL002) orthotopic xenograft models by ultrasound-guided injections into the adrenal gland and periadrenal space of immunocompromised mice. The technique was time efficient and reliable, with an overall engraftment of 95%, resulting in locally infiltrative NB tumors. Xenografts also exhibited distant metastasis to sites typical of NB (lymph nodes and cortical bone), a phenotype not reported in standard models. Additionally, as part of our ongoing collaborative efforts to develop modern surgical and molecular model systems that mimic the biological diversity of pediatric tumors, we expanded the technique to Ewing sarcoma (ES) renal subcapsular xenografts (TC32, A673, CHLA-25, or A4573). Grafting of primary tumors beneath the renal capsule has gained interest for its rapid engraftment and reliable metastatic spread (12). Like many types of cancer, metastasis is a powerful predictor of survival outcome in ES, therefore development of metastatic ES xenografts is critical for testing novel therapeutics. Both kidneys were accessible by ultrasound for percutaneous needle implantation of ES cells beneath the renal capsule, without opening the abdomen. All resulting ES renal subcapsular xenografts were locally infiltrative with bulky primary tumors. TC32 and A4573 were metastatic to lung parenchyma.

In this report, relevant cancer xenografts were established using ultrasound guidance for percutaneous tissue injections targeted to the adrenal gland for NB and to the renal subcapsule for ES. The technique was safe and efficient, providing a minimally invasive option for orthotopic and abdominal implantation of tumor cells for cancer xenograft development. The xenografts established demonstrated important human disease characteristics including a metastatic phenotype.

Materials and Methods

Cell culture. Human NB cell lines SH-SY5Y (ATCC), SK-N-BE2 (ATCC) and IMR32 (ATCC, Manassas, VA, USA) were grown in minimal essential medium, supplemented with 10% fetal bovine serum, 2 mM glutamine, 100 units/ml penicillin, and 100 μg/ml streptomycin (Thermo Fisher Scientific, Waltham, MA, USA). IMR32 medium was further supplemented with 1 mM pyruvate and 0.075% $NaHCO_3$. Human ES cell lines TC32, A673, CHLA-25, or A4573 (COGcell.org) were grown in RPMI medium, supplemented with 10% fetal bovine serum and 6 mM L-glutamine (Atlas Biologicals, Fort Collins, Co, USA). All cells were placed in an incubator at 37˚C and an atmosphere of 5% CO_2. Cells were sent to IDEXX RADIL BioResearch (Columbia, MO, USA) for authentication using CellCheck™, which checks for eight Short tandem repeat (STR) markers and amelogenin. The genetic profiles of each cell line were then confirmed by comparing to established reference profiles.

Generation of primary patient xenografts. With patient consent and assent, discarded tumor tissue from two patients with NB (UMNBL001 and UMNBL002) undergoing surgical resection for local control were obtained fresh and transported to the laboratory in MACS tissue storage solution (Miltenyi Biotec, Auburn, CA, USA). All patient samples and procedures were de-identified and handled in accordance with The University of Michigan Institutional Review Board approval (HUM 00052430) and guidelines. Surgically obtained tissue was disassociated using a tumor dissociator kit (Miltenyi Biotec TD Kit). Briefly, tumor was transferred to a culture dish containing RPMI buffer and minced to a paste-like consistency. Minced tumor was re-suspended in 5 ml of RPMI media and enzymes provided were added according to kit protocol. The tumor solution was then transferred to gentleMACS tubes (Miltenyi) and run on a gentleMACS dissociator (Miltenyi). The tumor cell suspension was incubated at 37˚C for 1 h on a rotating rack with intermittent trituration every 15 min. The cell suspension was transferred to a new tube and 10 ml of RPMI was added. Cells were centrifuged at 1,200 rpm for 5 min. The supernatant was suspended in 5 ml RPMI and passed through a 70 μm filter. Cells were then washed and centrifuged to collect a pellet that was re-suspended in RPMI. A mixture of 100 μl of cell suspension and matrigel (1:1) was then bilaterally injected into immunodeficient mice (NOD-SCID: Charles River Breeding Labs, Wilmington, MA, USA; or NOG-F: Taconic Biosciences, Hudson, NY, USA). The initial generation was termed passage 0 (P^0) and

engraftment was assessed at the subcutaneous flank as the primary endpoint for P^0. Subsequent generations were maintained P^1 through P^{10}. during which time the implantation sites were transitioned to direct adrenal gland injections for the current study.

For orthotopic adrenal gland implantation, a single-cell suspension from fresh tumor tissue was generated using the tumor dissociator procedures described above. P^1 through P^9 generations were utilized for the current studies. All procedures were by a protocol approved by the University Committee on Use and Care of Animals and animal care was overseen by the Unit for Laboratory Animal Medicine.

Generation of luciferase-expressing cell lines. To engineer luciferase-expressing cells, SH-SY5Y, SK-N-BE2, IMR32, UMNBL001, UMNBL002, TC32, A4573, A673, and CHLA-25 cells were virally transduced with Lenti-GF1 vector (University of Michigan, Vector Core, Ann Arbor, MI, USA). Lenti-GF1 lentiviral vector contains both green fluorescent protein (GFP) and firefly luciferase genes, which enable detection of both GFP and luciferase signals. After infection with Lenti-GF1 virus, luciferase cells were isolated based on GFP-positive signal on fluorescence-activated cell sorting (FACS) analysis. Luciferase gene expression was verified by microscopy *in vitro* before direct implantation into mice. Quantitation of luciferase signal was evaluated by Steadt-Glo Luciferase Assay kit according to the manufacturer's instructions (Promega, Madison, WI, USA).

Orthotopic xenograft injections. A Visual Sonics Vevo 2100 Ultrasound Imaging System (Toronto, Canada) was used for all ultrasound procedures and tumor measurements (University of Michigan Cardiovascular Center Research Core). Six to eight-week-old immunodeficient NOD-SCID (Charles River Laboratories) or NSG mice (The Jackson Laboratory, Bar Harbor, ME, USA) were anesthetized in an induction chamber using 2% isoflurane in O_2 delivered at 2 l/min and underwent an established surgical procedure for orthotopic injections directly into the adrenal gland or the peri-adrenal space. The adrenal gland and kidneys were located using high-resolution ultrasound guidance with a MS550D 22-55 MHz transducer. Luciferase-tagged human NB cell lines ($SH\text{-}SY5Y^{LUC}$, $SK\text{-}N\text{-}BE2^{LUC}$, $IMR32^{LUC}$) and luciferase-tagged fresh NB patient-derived tumor cells ($UMNBL001^{LUC}$, $UMNBL002^{LUC}$) at a density of 2.0×10^5 cells/μl were suspended in matrigel (BD Worldwide, Franklin Lakes, NJ, USA) at a 1:1 ratio. A 22-gauge catheter (BD Worldwide) was gently inserted through the skin and back muscle into the left adrenal gland or peri-adrenal space under direct visualization to provide a channel for tumor cell injections. After removal of the catheter hub, a chilled Hamilton syringe fitted with a 27-gauge bore needle (BD Worldwide) was loaded with 10 μl of the cell suspension and hand injected.

A similar technique was utilized for renal subcapsular ES injections. Luciferase-tagged human tumor cells ($TC32^{LUC}$, $A4573^{LUC}$, $A673^{LUC}$, or $CHLA\text{-}25^{LUC}$) were re-suspended in PBS and matrigel (1:1) at 2.0×10^5 cells/μl. Six- to eight-week-old NOD-SCID mice (Charles River Breeding Labs) were anesthetized. A 22-gauge catheter was gently inserted through the skin and back muscle beneath the left renal capsule using ultrasound guidance to provide a channel for tumor cell injections. Ten microliters of the cell suspension was then guided stereotactically through the catheter and positioned beneath the renal capsule using ultrasound visualization.

Tumor monitoring and Imaging. Animals were monitored weekly by bioluminescent imaging (up to 8 weeks), using an IVIS Spectrum *in vivo* imaging system (Perkin Elmer, Waltham, MA, USA). Imaging was performed at the Center for Molecular Imaging, University of Michigan. Mice were given an intraperitoneal injection of D-luciferin (4 mg/mouse; Promega) dissolved in PBS. Five minutes after luciferin injection, mice were anesthetized under 2% isoflurane in an induction chamber. Once adequate anesthesia was attained, animals were carefully transferred to the imaging platform and kept anesthetized with isoflurane *via* nose-cone inhalation. Parameters that were adjusted to control signal level were: Binning (resolution setting-corresponds to grouping of pixels into a larger super-pixel); exposure time (length of time the shutter is kept open, corresponds to light collected); and F/stop (lens aperture: controls the amount of light collected and depth of field); 1 (maximum light with low resolution) -8 (minimum light with high resolution). Initial imaging parameters were as follows: Large binning (high sensitivity/lower resolution), 30 second exposure time, 30 segments taken to determine peak of bioluminescence, 30 second delay between exposures and F/Stop 1. A total body standard region of interest (ROI) that encompassed the entire body, including both primary and distant metastatic tumors, was calculated using Living Image 4.3 software (Perkin Elmer). Bioluminescence, expressed as radiance, was quantified as $p/s/cm^2/sr$.

Ultrasound imaging was also utilized to monitor weekly tumor growth. Mice were anesthetized with 2% isoflurane in an induction chamber, then transferred to the examination table and maintained on isoflurane anesthesia through nose cone inhalation. Visual Sonics Vevo 2100 Imaging System was used to capture images. Depending on the size of tumor, transducers varied from MS550D 22-55 MHz probe (baseline measurement) to MS400 18-38 MHz probe (medium-sized tumors), to MS250 13-24 MHz or MS200 9-18 MHz (larger tumors). Tumor location, size, and relation to the adrenal gland and kidney were tracked. Tumor volume was calculated (mm^3) using the MS250 13-24 MHz or MS200 9-18 MHz probes.

Histopathological examination. All xenografted animals and resultant tumors were examined and characterized histologically by a board-certified veterinary pathologist (MJH) at the *In Vivo* Animal Core (University of Michigan). Primary xenografted tumors, along with tissues typical of NB metastasis (lymph nodes, cortical bones, liver, lungs) or ES (lung, lymph nodes, cortical bones) were collected and characterized histologically by routine hematoxylin and eosin (H&E) staining. Characteristic tumor-specific proteins (tyrosine hydroxylase, CD99) were also assessed using immunohistochemistry. Paraffin blocks were sectioned at 4 μm and slides were labeled with antibodies to tyrosine hydroxylase (mouse monoclonal, 1:100; Sigma, St. Louis, MO, USA) or CD99 (mouse monoclonal; 1:100; DAKO, Carpinteria, CA, USA). Following antigen retrieval, quenching of endogenous peroxidase, and rodent block reagents (Biocare, Concord, CA, USA), sections were incubated with primary antibodies and washed. Following washing, polymer horseradish peroxidase conjugated secondary antibodies (Biocare) were applied. Negative controls were obtained by substitution of the primary antibody with Universal Negative reagent (Biocare). Following washing, 3,3-diaminobenzidine (DAB) was applied to visualize all reactions, and slides were counterstained with hematoxylin. The sections were dehydrated through graded alcohols, immersed in xylene, and mounted with coverslips.

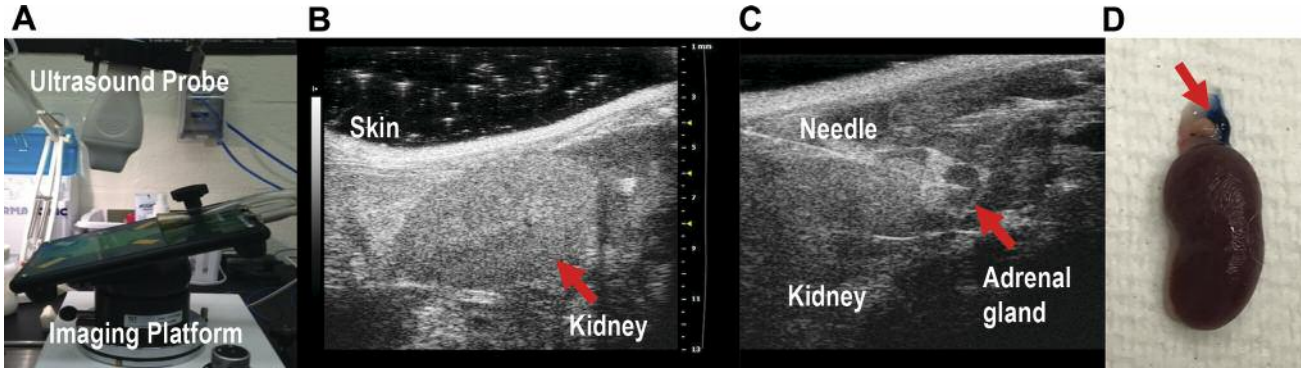

Figure 1. *A: High-resolution ultrasound imaging with a 22-55 MHz transducer visualized murine abdominal organs and allowed adrenal gland and peri-adrenal space implantation of neuroblastoma (NB) cells. B: The left kidney was identified and utilized as an anatomical landmark. C: The adrenal gland was depicted cranial to the kidney and appeared as a discrete round hypoechoic structure. Ultrasound-guided needle implantation of human NB cells into the adrenal gland is shown. D: For initial studies, a mixture of matrigel and methylene blue dye were utilized to assess results of injection procedures. A representative ex vivo image is shown an of the left adrenal gland and kidney with both matrigel and methylene blue dye at the lateral adrenal capsule edge and peri-adrenal space.*

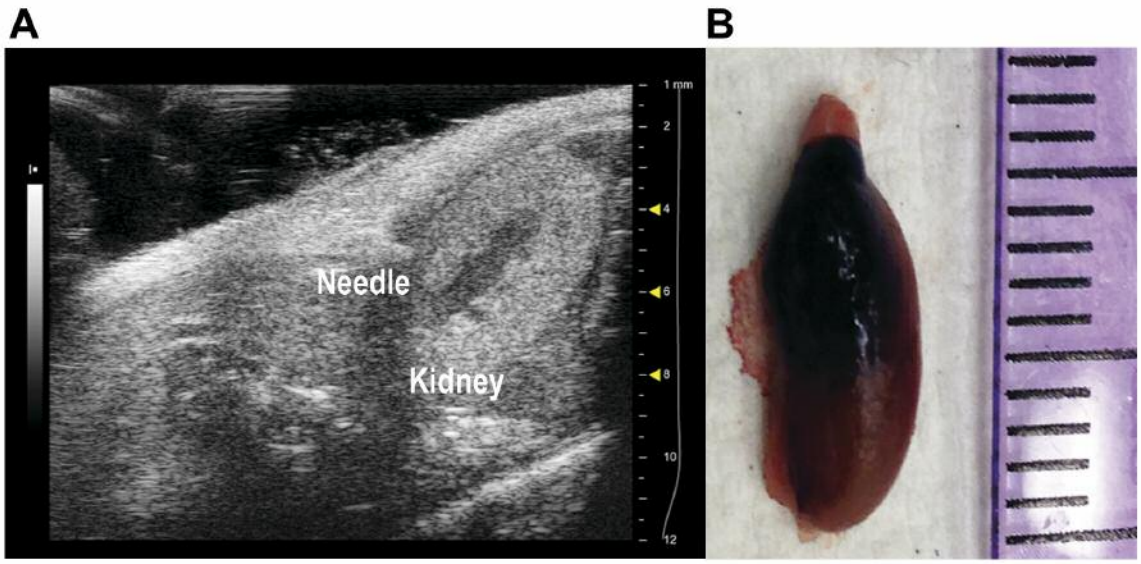

Figure 2. *Renal subcapsular implantation of Ewing sarcoma (ES) cells. A: Single-cell suspension of ES cells were implanted beneath the renal capsule using ultrasound-guided needle injections. B: Renal subcapsular injection was first demonstrated using methylene blue dye and matrigel. Representative ex vivo image of left kidney post-injection is shown.*

Results

High-resolution ultrasound allowed localization of murine abdominal organs and injection of human pediatric solid tumor cells without open surgery. Micro-ultrasound with a high-resolution, high-frequency digital imaging platform (Vevo 2100. MS550D 22-55 MHz probe; Figure 1A) allowed for consistent visualization of mouse abdominal viscera and vasculature including both adrenal glands, spleen, liver, both kidneys, intestines, and urinary bladder. As in humans, the adrenal glands in the mouse are depicted as paired organs, located cranial to the kidneys, and appear as small round hypoechoic structures on ultrasound. The adrenal glands ranged in size from 2 to 3.5 mm, and appeared on ultrasound as solid organs with a circular target-like sign above the kidneys. We utilized the left adrenal gland for orthotopic injections given its

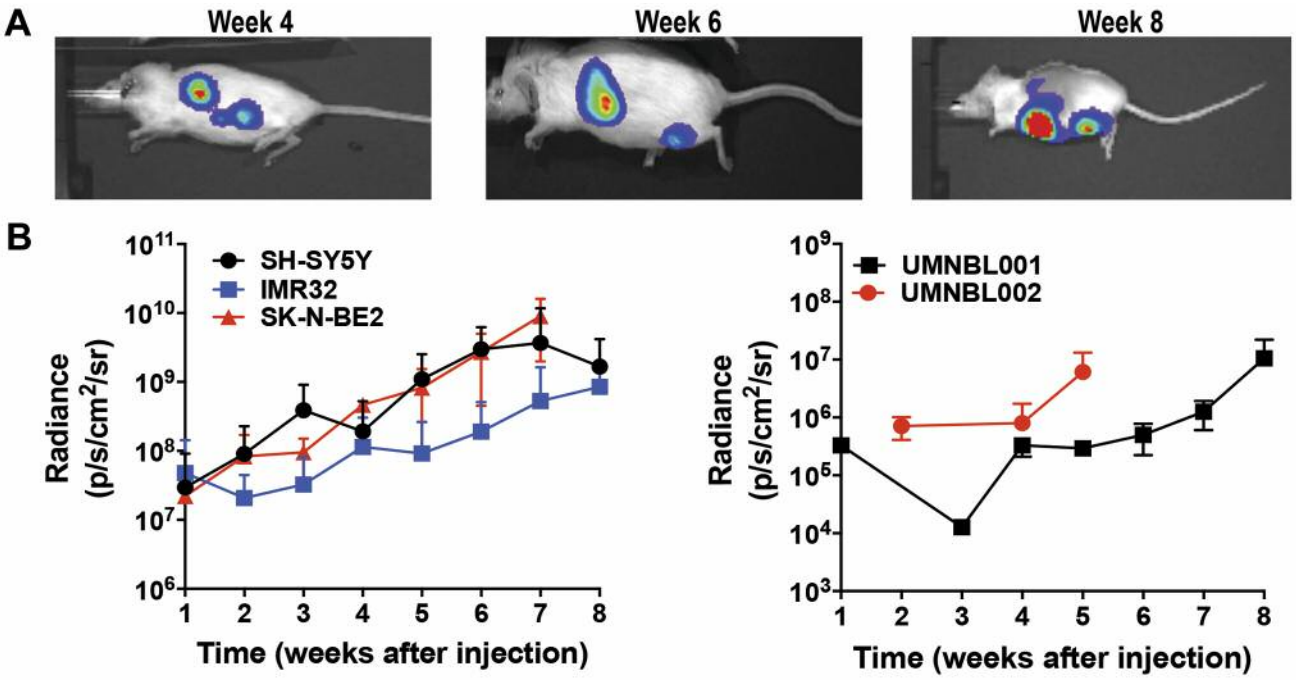

Figure 3. *Bioluminescence in vivo imaging was used to monitor sequential tissue-directed neuroblastoma (NB) tumor growth. A: Adrenal xenografts established from human NB cells had engraftment and growth rates monitored through eight weeks. B: Standard region of interest was determined at maximal bioluminescence signal and utilized to define the average radiance expressed as p/s/cm²/sr at each time point. NB cell lines (SH-SY5Y, IMR32, SK-N-BE2) had the same initial starting radiance and consistently increased from baseline over time. NB patient-derived xenografts (UMNBL001, UMNB002) also showed increased radiance with time although overall growth patterns varied.*

larger size compared to the right adrenal gland, and safe distance from the inferior vena cava and aorta (Figure 1B and C). In order to confirm the accuracy of ultrasound localization of the adrenal gland, initial studies were conducted in which a methylene blue dye and matrigel mixture (1:1) was percutaneously injected into the adrenal gland and peri-adrenal space using ultrasound guidance. Abdominal exploration and necropsy confirmed inoculation and local maintenance of the blue dye and matrigel mixture within the adrenal gland and the attached peri-adrenal fat, without spillage into the kidney or surrounding organs (Figure 1D).

We first used three human NB cell lines (IMR32, SH-SY5Y, SK-N-BE2) for direct orthotopic injections into the adrenal gland or peri-adrenal space (n=3-13 mice per group). This location was selected because most NB tumors are found in the retroperitoneum involving the adrenal gland and suprarenal sites. The selected cell lines have been shown to form tumors in murine models and were derived from high-risk human NB with *MYCN* amplification (IMR32 and SK-N-BE2), 1p36 loss of heterozygosity (LOH) (SH-SY5Y), or *TP53* mutation (SK-N-BE2). These genetic alterations are common to metastatic NB tumors and predict treatment resistance and poor survival outcomes.

In addition to NB cell lines maintained in culture, fresh patient-derived NB tumor cells (UMNBL001, UMNBL002) were also utilized for ultrasound-guided implantation. UMNBL001 was obtained from a 6-year-old patient undergoing resection of a retroperitoneal mass of relapsed NB. The patient originally presented with a retroperitoneal mass that was metastatic to lymph nodes and cortical bone at multiple thoracic and lumbar vertebrae. He had biopsy-confirmed poorly differentiated NB with unfavorable histology (International Neuroblastoma Staging System, Stage 4), non-*MYCN* amplified with LOH at 1p. His therapy consisted of multi-agent chemotherapy, complete gross surgical resection, autologous stem cell transplant with carboplatin/etoposide/melphalan conditioning, radiation to the retroperitoneum, and chimeric antibody therapy (ch 14.18). UMNBL002 was obtained from a 2-year-old patient who presented with a large adrenal mass that was widely metastatic to regional and pelvic lymph nodes, liver, cortical bone, and bone marrow. Urine catecholamines were elevated and the biopsy confirmed NB with *MYCN* amplification and multiple segmental chromosomal abnormalities. The patient had received four cycles of induction chemotherapy with good response and underwent total gross resection followed by myeloablative chemotherapy and autologous stem cell transplant.

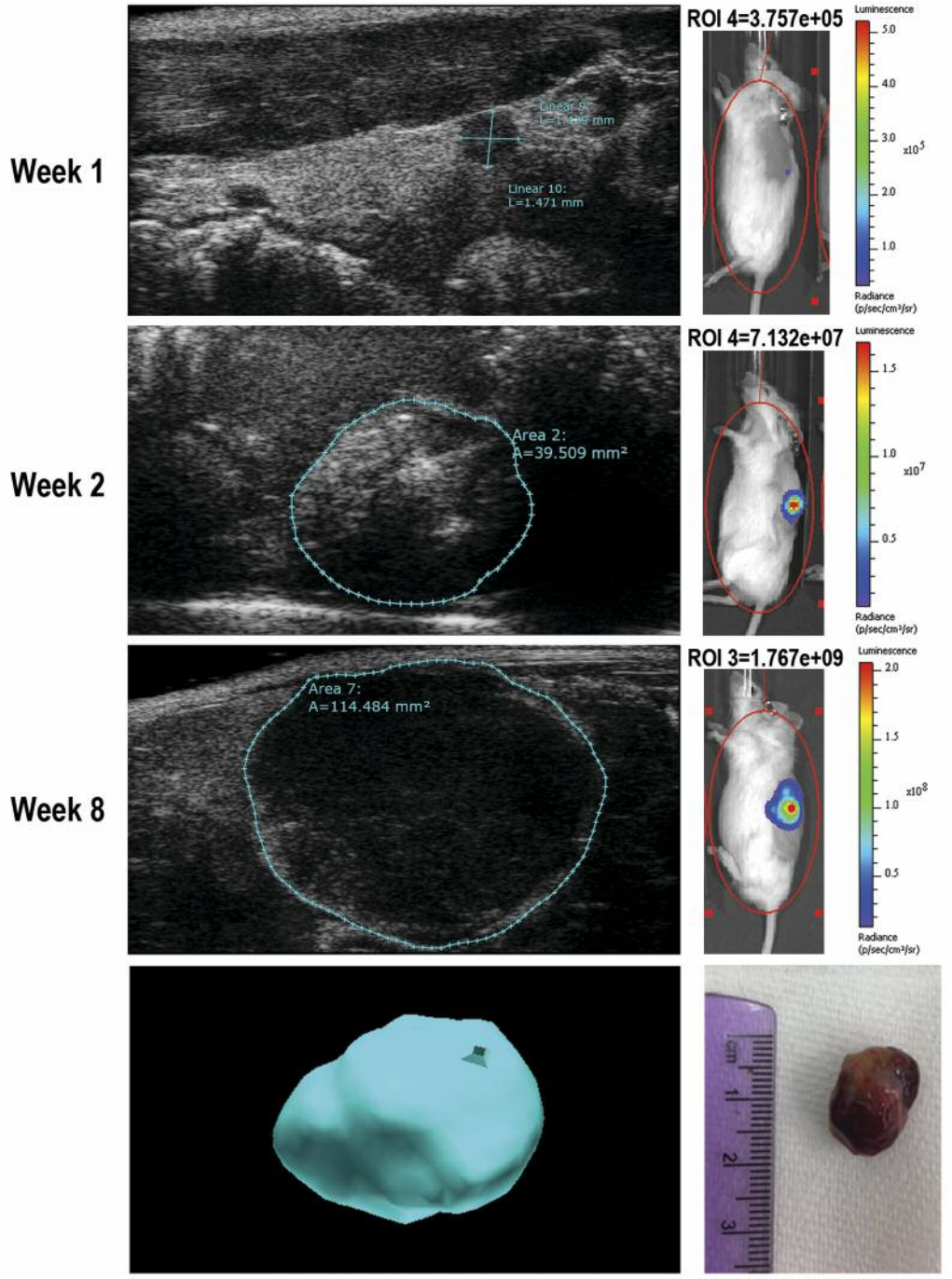

Figure 4. *Ultrasound imaging was also utilized to monitor in vivo tumor growth for neuroblastoma (NB) orthotopic adrenal xenografts. Representative ultrasound and corresponding bioluminescence images at weeks one, two, and eight are shown. Evidence of engraftment was detected by week one in both imaging modalities. Tumor area (mm^2) was monitored and increased with each time point from baseline. 3D ultrasound images (bottom panel) recapitulated physical characteristics of excised tumors at necropsy.*

Rather than open laparotomy, single-suspension luciferase-labeled NB cells (SH-SY5Y^{LUC}, SK-N-BE2^{LUC}, or IMR32^{LUC}) or fresh NB patient-derived tumor cells (UMNBL001^{LUC}, UMNBL002^{LUC}; after P^0 subcutaneous expansion) were hand-injected percutaneously under direct visualization into the adrenal gland of immunocompromised (NOD/SCID or NSG) mice. The abdominal wall skin and musculature were not incised. There were no complications

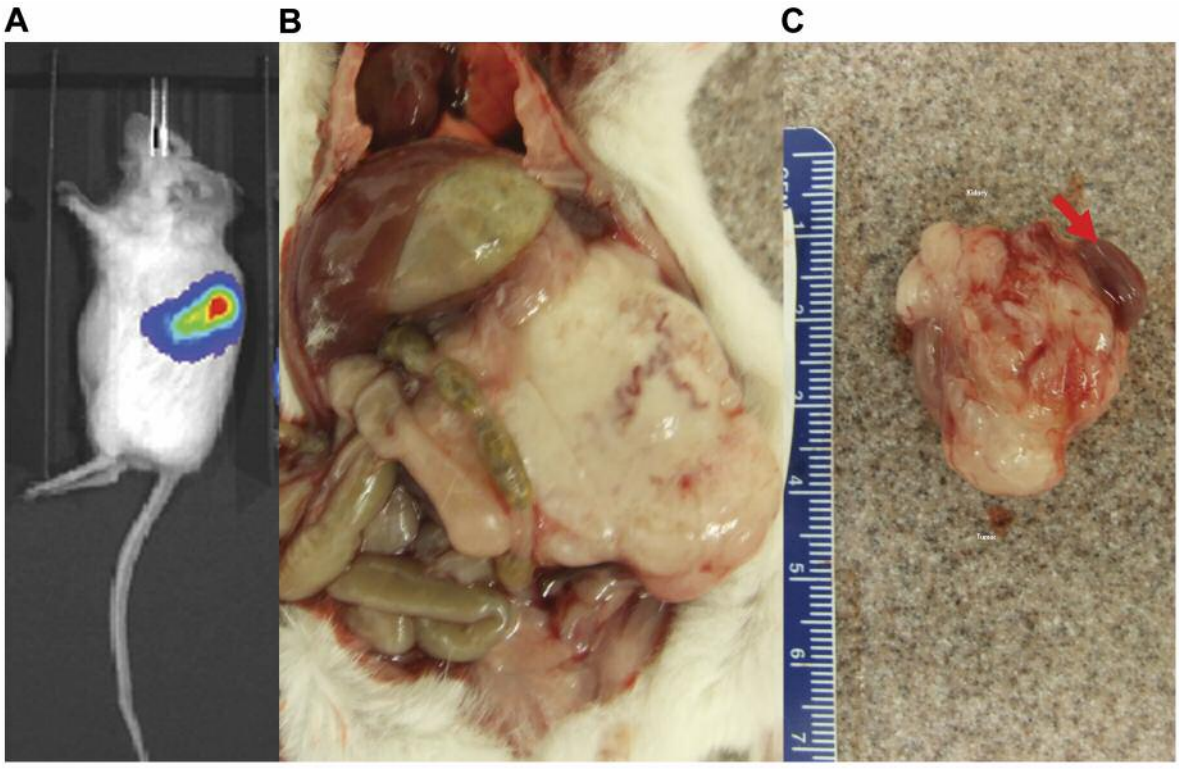

Figure 5. *Ewing sarcoma (ES) cell lines implanted by ultrasound-guidance formed renal subcapsular xenografted tumors. A: Bioluminescence imaging was used to track tumor radiance. Necropsy (B) with tumor excision (C) revealed that animals developed lobulated locally invasive tumors that distorted surrounding abdominal structures.*

or bleeding events. Post-injection, animals were awakened and returned to their cages where they were observed to return to normal functional activities within 15 minutes, without any prolonged recovery periods. There was no morbidity or mortality associated with ultrasound or needle injection procedures.

The technique was then modified for ES cell lines to establish a reliable model of ES metastasis for collaborative preclinical studies. Renal subcapsular implantation of tumor cells has recently been described as a promising model for study of spontaneous metastasis of ES, a clinical entity not easily modeled *in vivo* (12). The renal subcapsular graft site reliably forms xenografts that retain major histological features of the original cancer for a variety of cell lines (13). Compared to subcutaneous implantation and other orthotopic sites, renal subcapsular engraftment of ES has a higher tumor take rate and rapidly forms spontaneous distant metastases, likely related to the robust vascularity of the engraftment site (14). Without opening the abdomen or exteriorizing the kidney, single-suspension luciferase-labeled ES cells ($TC32^{LUC}$, $A4573^{LUC}$, $A673^{LUC}$, or $CHLA\text{-}25^{LUC}$) were percutaneously injected beneath the renal capsule under direct visualization using ultrasound guidance (Figure 2A and B, n=5 mice per group). TC32 (*EWS/FLI1* fusion oncogene, *P16* null, *P14* null), A4573 (*EWS/FLI1* fusion oncogene), A673 (*EWS/FLI1* fusion oncogene, *TP53* non-functional, *P16* null, *P14* null), and CHLA-25 (*EWS/ERG* fusion oncogene, *TP53* non-functional) cells were selected because they have been genetically well-characterized and commonly utilized in metastatic xenograft models of ES (15-18). Both kidneys in NOD/SCID mouse were consistently visualized with high-resolution ultrasound and unilateral renal subcapsular ES cell injections were performed by percutaneous injection. There were no complications or the need for extended recovery periods. There were no procedural hematomas or bleeding events. After injection, mice were returned to their cages where they were noted to resume pre-procedural activities within 15 minutes. Identification and localization of kidneys and surrounding structures by ultrasound allowed safe and efficient percutaneous injection of ES cells, a technique not previously utilized to establish ES xenografts for preclinical studies.

In vivo imaging monitored sequential NB and ES tissue-directed tumor growth in xenografts. Bioluminescence was utilized to localize and quantitate early to late-stage tumor growth *in vivo*, with real-time evaluation of tumor burden

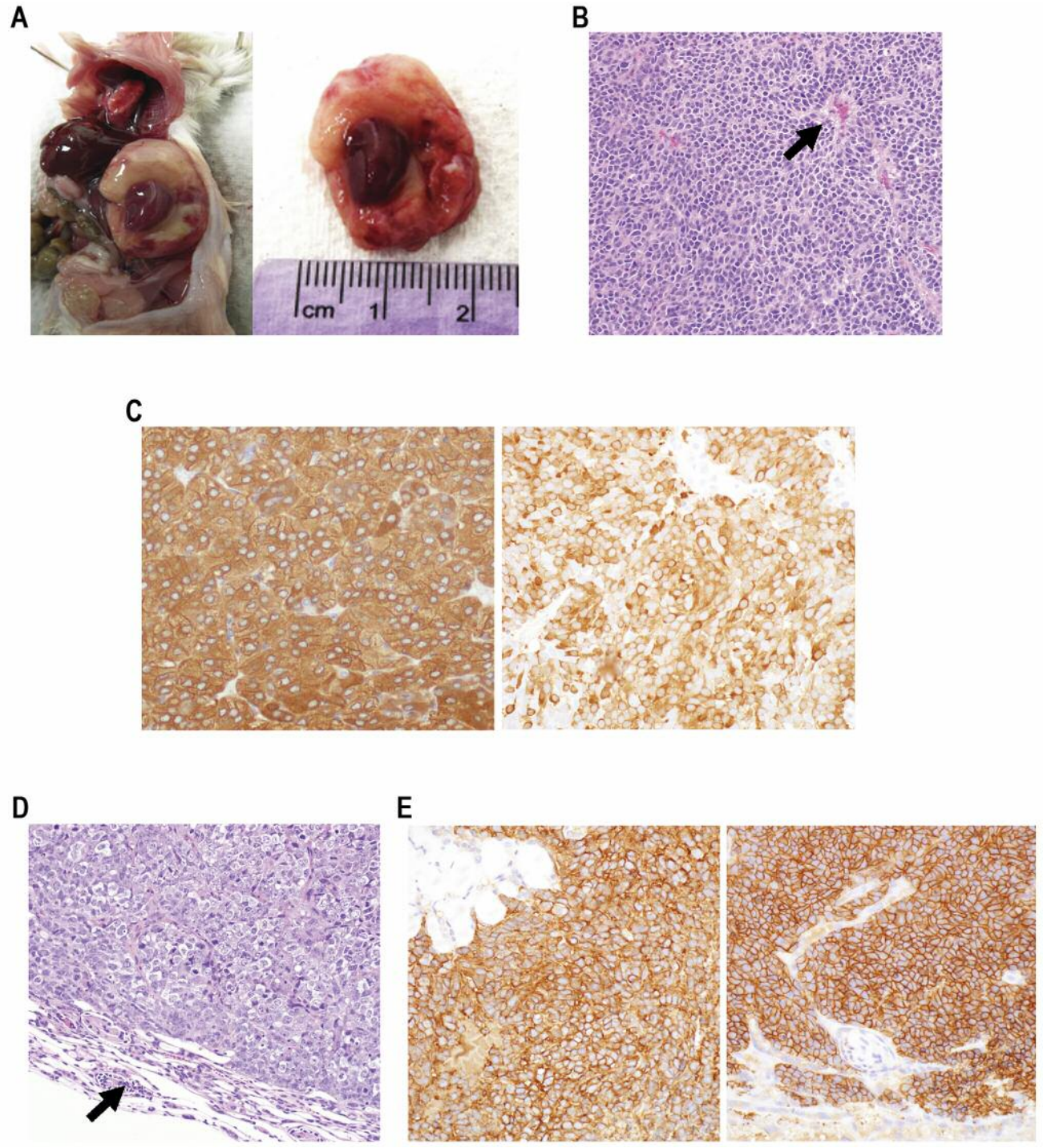

Figure 6. *Gross and histological characterization of neuroblastoma (NB) and Ewing sarcoma (ES) xenografts. A: At necropsy, NB-xenografted animals were found to have primary tumors at the adrenal and peri-adrenal gland sites that were locally infiltrative and distorted the adjacent kidney, hepatic parenchyma, diaphragm, pancreas, and lumbar musculature. B: Microscopically (20×), adrenal site tumors had morphological features of human NB. Primary tumors maintained a neuroendocrine phenotype with poorly differentiated round cells, which formed pseudorosettes palisading around blood vessels (arrow). C: Neoplastic cells showed positive immunoreactivity for the NB marker tyrosine hydroxylase (40×; positive control staining shown in the left panel; 1:100). D: Microscopic analysis of primary ES-xenografted tumors were histologically consistent with locally infiltrative ES (40×). Tumors were composed of poorly differentiated epithelioid cells within a fibrovascular stroma. The primary tumor xenografts effaced and compressed the adjacent kidney (arrow). E: Immunohistochemistry for ES tumor marker CD99 showed strong membrane immunoreactivity (40×; positive control staining shown in the left panel; 1:100).*

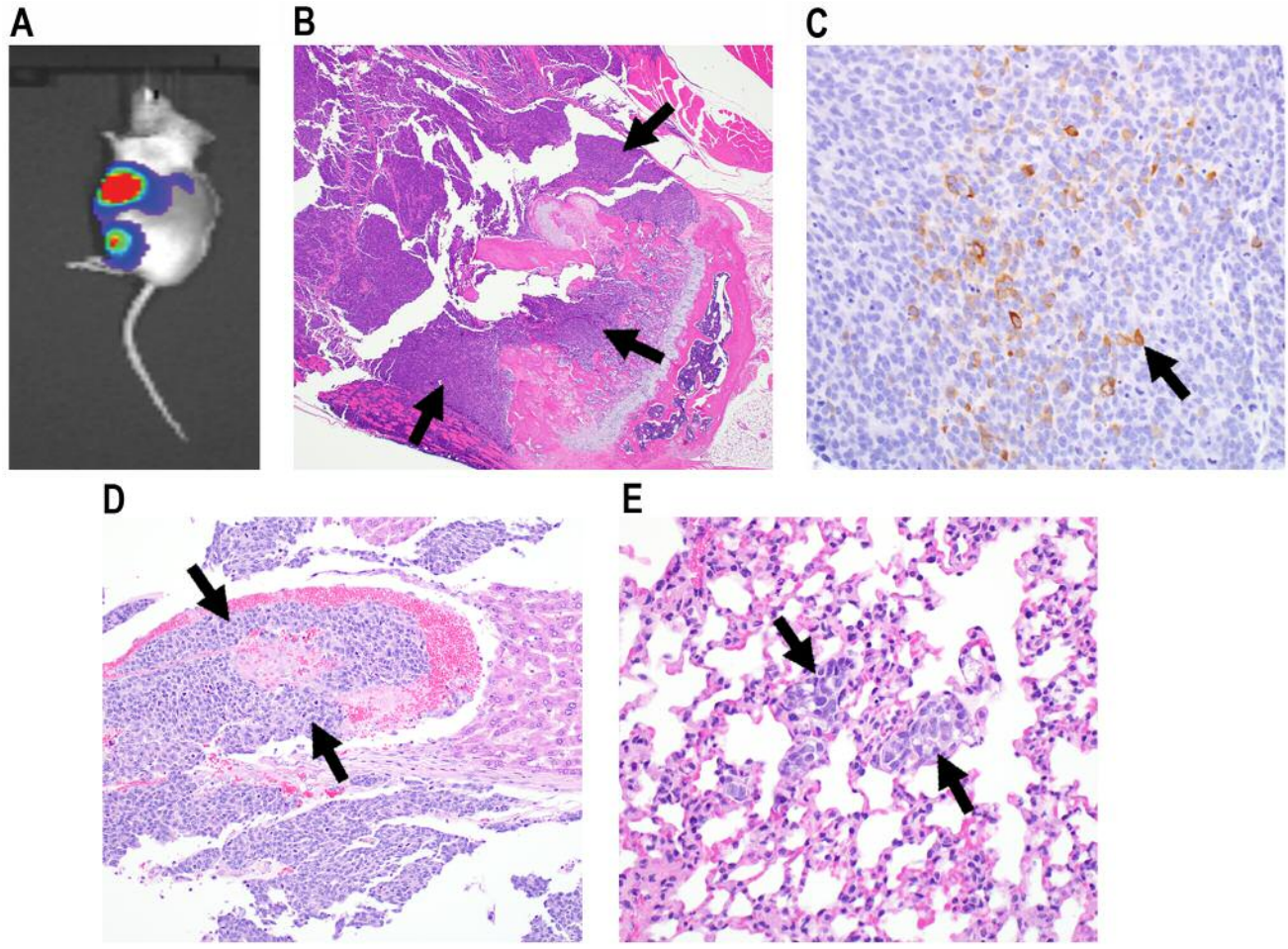

Figure 7. *Distant metastases were demonstrated in xenografts established by ultrasound-guided tissue implantation. A: Bioluminescence signal detected the primary adrenal tumor shown with separate foci in the region of the left lower extremity. B: Microscopic analysis (4×) demonstrated metastasis within the proximal femur effacing the marrow cavity of the metaphysis and proximal diaphysis (arrows), replacing cortical bone and adjacent skeletal muscle. C: Immunohistochemistry for tyrosine hydroxylase showed positive cytoplasmic immunoreactivity in metastatic neuroblastoma (NB) cells (40×). D: Representative microscopy from patient-derived orthotopic xenograft (UMNBL002) with distinct metastatic foci (arrows) invading hepatic vasculature and parenchyma (20×). E: NB tumor cell emboli were present within the pulmonary vasculature and micrometastases (arrows) were visualized within the pulmonary parenchyma (40×).*

and metastasis. Compared to fluorescent imaging, bioluminescence imaging is more sensitive in evaluating tumor growth in early stages prior to detection by palpation. After stable transfection of tumor cells with luciferase, the reaction of luciferase with its substrate luciferin emits photons that are detected by photon-counting cameras (19). Photon emission is proportional to the number of luciferase-tagged cells present and enhances with tumor growth. Luciferase and luciferin have not been shown to have toxic or functional effects in expressing cells (19). Exogenous luciferin was administered by intraperitoneal injection and animals were imaged within five minutes. For all NB xenografts, mice were analyzed for evidence of tumor engraftment post-injection as detected by localized bioluminescence signal. Standard ROI was determined at maximal bioluminescent signal and utilized to define the average radiance at each time point. Tumor engraftment and growth were monitored by Xenogen imaging for up to 8 weeks (Figure 3). Adrenal xenografts established from NB cell lines (IMR32, SH-SY5Y, SK-N-BE2) reached tumor radiance of 10^8 p/s/cm^2/sr by 4 weeks, while patient-derived orthotopic xenografts (UMNBL001, UMNBL002) also showed aggressive growth rates, reaching 10^6 to 10^8 p/s/cm^2/sr between 4 to 8 weeks. All cell lines had the same initial starting radiance, yet IMR32 tumors had a slower, more gradual growth rate compared to SH-SY5Y and SK-N-

BE2 tumors. Localized bioluminescent signal of 10^6 to 10^8 p/s/cm^2/sr has been reported as an indicator of tumor engraftment in the adrenal space adequate to initiate preclinical studies of NB (11). Overall engraftment rates ranged from 62% to 90% (Table I).

Bioluminescent imaging has been found to correlate with linear volume measurements when NB tumors are small, but *in vivo* ultrasound measurements may be more consistent when tumors are large (11). We found that in addition to large tumor burden, bioluminescent signaling may also be inconsistent after multiple generations and *ex vivo* tumor passaging in patient-derived xenografts. Given this, we determined the feasibility of ultrasound imaging for monitoring *in vivo* tumor growth in this model. A cohort of five UMNBL002 and five IMR32 orthotopic xenografts were imaged bi-weekly after initial injection procedures. Engrafted tumors were detectable early by diagnostic ultrasound and remained consistent throughout all growth phases (Figure 4). Early tumors were detected as enlarging hypoechoic and anechoic structures at the adrenal space, superior to the kidney and abutting surrounding structures at the midline. Primary tumor area measurements derived from NB cell line xenografts ranged from 5.46 mm^2 to 875 mm^2, while patient-derived tumor area ranged from 45.99 mm^2 to 1,036 mm^2.

For ES xenografts, the cell lines tested readily formed xenografts with aggressive growth rates at the sites of kidney injections. A4573, A673, CHLA-25, and TC32 cells were tested for feasibility, resulting in locally invasive primary tumors with an overall engraftment rate of 85% (n=5 mice per group, Table II). Weekly bioluminescence imaging demonstrated that ES cell line xenografted tumors reached adequate tumor radiance (defined as >10^6 p/s/cm^2/sr) within 25 days (Figure 5).

Gross and histological characterization of NB and ES xenografts. Adrenal and renal subcapsular tumors that developed after engraftment were analyzed at necropsy and histologically for characterization of the primary tumor and evaluation for the presence of metastases. For NB tumors, necropsy revealed that animals developed primary tumors at the adrenal gland sites that were locally invasive and distorted adjacent structures including the kidney, diaphragm, hepatic parenchyma, pancreas, and lumbar musculature (Figure 6A). Microscopically, adrenal xenograft tumors had morphological features that were histologically consistent with infiltrative NB. The primary tumors maintained a neuroendocrine phenotype, comprising an expansive proliferation of sheets and clusters of poorly differentiated neoplastic cells, that often formed pseudorosettes and palisaded around blood vessels with multifocal to coalescing zones of serpentine necrosis (Figure 6B). Neoplastic cells were ovoid to stellate cells, with finely clumped marginated chromatin and 1-3 prominent nucleoli and a brisk mitotic rate. All tumors showed positive cytoplasmic immunoreactivity for the NB marker tyrosine hydroxylase (Figure 6C). Non-specific background staining was not observed.

Table I. *Adrenal engraftment rate for neuroblastoma orthotopic xenografts.*

Adrenal engraftment	
Cell Line	Number of mice/Total mice (%)
IMR32	8/13 (62%)
SH-SY5Y	7/9 (78%)
SK-N-BE2	3/3 (100%)
UMNBL001	4/5 (80%)
UMNBL002	9/10 (90%)

Table II. *Renal subcapsular engraftment rates for Ewing sarcoma xenografts.*

Renal subcapsular engraftment	
Cell Line	Number of mice/Total mice (%)
A4573	3/5 (60%)
A673	4/5 (80%)
CHLA-25	5/5 (100%)
TC32	5/5 (100%)

For ES renal subcapsular xenografts, tumors were morphologically and histologically consistent with locally infiltrative ES. The primary tumor xenografts effaced 35% to 99% of the kidney and adhered to the surrounding lumbar skeletal musculature. Most tumors were found to have direct extension into the surrounding liver and pancreatic parenchyma, and infiltrated within the mesenteric fat. Each xenografted tumor was composed of an unencapsulated proliferation of poorly differentiated epithelioid cells within a scant fibrovascular stroma (Figure 6D). The cells were angular to ovoid, with scant to moderately eosinophilic vacuolated cytoplasm and hyperchromatic nuclei with clumped marginated chromatin. There was variable central necrosis characterized by loss of cellular architecture, and a high mitotic rate. Immunohistochemistry for the ES tumor marker CD99 showed strong membrane immunoreactivity in 100% of tumor cells examined (Figure 6E).

To begin to evaluate the capacity for metastases in these newly established xenografts, sections of lung, liver, right kidney, urinary bladder, mesenteric and pelvic lymph nodes, spleen, pancreas, and select bones (femur, tibia, vertebral column, and sternum) were examined microscopically from xenografted animals. Distant metastases were demonstrated in both NB and ES xenografts. For NB cell line orthotopic xenografts, micrometastases were identified in the lung parenchyma, mesenteric/pelvic lymph nodes, and cortical

bone (femur) (Figures 7A-C). Although bioluminescent imaging occasionally detected metastatic disease prior to necropsy, this was not a consistent finding. The metastatic rate was 14% for SH-SY5Y, 33% for SK-N-BE2, and 12.5% for IMR32 tumors. Patient-derived orthotopic xenograft UMNBL002 demonstrated the most consistent and robust metastatic patterns, with metastases found in both xenografts examined (100%). Significantly, discrete metastatic foci were distributed within lung parenchyma and invading hepatic vasculature and parenchyma, replicating features of the original patient's tumor (Figures 7D and E). These findings suggest that patient-derived orthotopic xenografts closely replicate biologic phenotypes of the original tumor. For ES renal subcapsular xenografts, TC32 (40%) and A4573 (33%) exhibited metastases to lung parenchyma.

Discussion

Predictive animal models are needed for diagnostic and treatment advancements for children with metastatic NB and ES, two of the most treatment-resistant solid tumors. In general, there has been poor correlation between preclinical testing of new compounds and therapeutic efficacy in clinical trials. Standard xenografts are cell-line derived from subcutaneous flank engraftment or from kidney capsule implantation *via* open surgery. Compared to subcutaneous tumors, orthotopic sites are more likely to recapitulate the tumor microenvironment and form vascularized xenografts that spontaneously metastasize (20). In order to establish reliable preclinical models that most consistently exhibit biologic features seen in clinical practice, we set out to develop NB and ES metastatic xenografts utilizing ultrasound for implantation of tumor cells. We expanded the method to include a broad set of human NB cell lines, fresh samples from patient-derived NB tumors, and ES cell lines. Ultrasound localization of intra-abdominal organs was utilized for percutaneous cell injections to avoid associated morbidity and time constraints of open mouse surgery.

Tumors survive by genomic instability, dysregulated cellular mechanics and integration into the host environment (21). With the advent of more targeted therapies for cancer treatment, understanding the microenvironment and relation of tumors to their surroundings has become a stepping stone to the development of anticancer therapies (1). In line with this, improvements in modern xenograft models are required to enable investigators to analyze and understand tumor biology in the context of the microenvironment and native tissue surroundings. Patients with metastatic disease remain the most challenging treatment groups for which new therapies are urgently needed, therefore the development of xenograft models that mimic human disease and metastatic phenotypes is critical for preclinical studies testing combination therapies, novel agents, or new targeted therapies.

Subcutaneous injection of tumor cells is the traditional approach utilized for NB and ES xenografts. The standard flank injection methods provide technically simple and reproducible models of primary tumors that are easily tracked by caliper measurements. The disadvantages to this method are the lack of tumor metastasis and absence of a 'native' tumor environment. The murine microenvironment has now been shown to mimic the natural tumor environment, facilitating its natural growth and angiogenesis patterns (22). This has facilitated the preference of orthotopic xenograft models for novel preclinical drug testing in pediatric tumors such as NB and ES.

In this study, an ultrasound-guided minimally-invasive method for introduction of tumor cells was utilized for orthotopic implantation, rather than open surgery. The technique was efficient, with up to 10 mice injected per 2-hour session. We found that mice had fast recovery times of less than 15 minutes without procedure-related morbidity or mortality. Moreover, abdominal organ identification and tissue targeted implantation of cells was reliable and precise, with high engraftment rates and distant metastases found for both NB and ES xenografts. This approach may serve as a feasible alternative to open and invasive methods of establishing cancer xenografts that are often limited by long and tedious surgical procedures. Standard open techniques carry high morbidity and are particularly challenging for abdominal organ access including the adrenal gland and kidneys. Ultrasound was also accurate for monitoring tumor growth *in vivo*. The current data suggests that ultrasound may enhance monitoring of orthotopic and abdominal xenografted tumors in both early and late stages of growth compared to bioluminescence alone.

Patient-derived tumor cells for xenograft development offer a unique opportunity to monitor characteristics of the primary tumor without the influence of culture media and potential genetic divergence. Significantly, these data provide two newly established NB patient-derived orthotopic xenografts (UMNBL001, UMNBL002), a rare model for future preclinical therapeutic testing and molecular studies. This model, similar to other patient-derived cancer models had overall high tumor engraftment and locally invasive growth at the orthotopic site (23). UMNBL002 patient-derived orthotopic xenografts faithfully produced robust, infiltrative tumors that were metastatic to lung and lymph nodes. In line with previously described models, patient-derived xenografts remain limited by potential variability in tumor uptake times and metastatic rates, as evidenced by failure of UMNBL001 xenografts to produce metastases despite 80% engraftment of robust primary tumors. This may be due to differences in treatment effects and biological characteristics of the original tumors. UMNBL001 came from a heavily treated relapsed NB tumor that was non-*MYCN* amplified, while UMNBL002 was obtained at the initial

resection of a widely metastatic *MYCN*-amplified tumor. The effects of these biological differences on the establishment of patient-derived orthotopic xenografts are unknown and form the basis for future investigations. Future studies will also be directed at further optimizing the technique to enhance metastatic potential and tracking metastatic disease by ultrasound. This will include utilizing increased cell numbers for implantation and enriching the cell population for rapidly proliferating and viable tumor cells.

These data indicate that ultrasound-guided percutaneous implantation of tumor cells is a reliable method to establish both adrenal NB and ES renal capsular xenografts with histological and clinical features similar to human disease phenotypes. Tissue-targeted engraftment of tumors will facilitate studies that advance understanding of tumor microenvironment and recapitulate complexities of metastatic spread. These models may provide significant advantage for investigational studies designed to improve pediatric NB and ES patient outcomes, and provide relevant framework for preclinical drug discovery.

Conflicts of Interest

The Authors have no financial or other conflicts of interest.

Acknowledgements

This work was financially supported in part by funds from the Robert Wood Johnson Foundation/Amos Medical Faculty Development Program (to EAN), The Alfred Taubman Medical Research Institute/Edith Briskin Emerging Scholar Program (EAN), and the Section of Pediatric Surgery, The University of Michigan and the NIH grant U54 CA168512 (ERL). The Authors wish to thank Kimber Converso-Baran and Dr. Marcus Jarboe for assistance with technical aspects of ultrasound injection procedures and the Visual Sonics Vevo 2100 Imaging System. We thank Paul Trombley for his help with graphics for the figures. We also thank the Department of Radiology at The University of Michigan for the use of The Center for Molecular Imaging and the Tumor Imaging Core which are supported in part by Comprehensive Cancer Center NIH grant P30 CA046592. The University of Michigan Physiology Phenotyping Core that is supported in part by grant funding from the NIH (OD016502) and the Frankel Cardiovascular Center. We thank Tammy Stoll, Dr. Rajen Mody and the Mott Solid Tumor Oncology Program. Our patients and families are gratefully acknowledged for their inspiration, courage, and ongoing support of our research.

References

1 Sanmamed MF, Chester C, Melero I and Kohrt H: Defining the optimal murine models to investigate immune checkpoint blockers and their combination with other immunotherapies. Ann Oncol *27*: 1190-1198, 2016.

2 Fidler IJ and Hart IR: Biological diversity in metastatic neoplasms: origins and implications. Science *217*: 998-1003, 1982.

3 Bibby MC: Orthotopic models of cancer for preclinical drug evaluation. Eur J Cancer *40*: 852-857, 2004.

4 Killion JJ, Radinsky R and Fidler IJ: Orthotopic models are necessary to predict therapy of transplantable tumors in Mice. Cancer Metastasis Rev *17*: 279-284, 1998.

5 Daniel VC, Marchionni L, Hierman JS, Rhodes JT, Devereux WL, Rudin CM, Yung R, Parmigiani G, Dorsch M, Peacock CD and Watkins DN: A primary xenograft model of small-cell lung cancer reveals irreversible changes in gene expression imposed by culture *in vitro*. Cancer Res *69*: 3364-3373, 2009.

6 Smith MA, Seibel NL, Altekruse SF, Ries LAG, Melbert DL, O'Leary M, Smith FO and Reaman GH: Outcomes for children and adolescents with cancer: challenges for the twenty-first century. J Clin Oncol *28*: 2625-2634, 2010.

7 Bosse KR and Maris JM: Advances in the translational genomics of neuroblastoma: From improving risk stratification and revealing novel biology to identifying actionable genomic alterations. Cancer *122*: 20-33, 2016.

8 Khanna C, Jaboin JJ, Drakos E, Tsokos M and Thiele CJ: Biologically relevant orthotopic neuroblastoma xenograft models: Primary adrenal tumor growth and spontaneous distant metastasis. In Vivo *16*: 77-85, 2002.

9 Stewart E, Shelat A, Bradley C, Chen X, Federico S, Thiagarajan S, Shirinifard A, Bahrami A, Pappo A, Qu C, Finkelstein D, Sablauer A and Dyer MA: Development and characterization of a human orthotopic neuroblastoma xenograft. Dev Biol *407*: 344-355, 2015.

10 Jäger W, Moskalev I, Janssen C, Hayashi T, Gust KM, Awrey S and Black PC: Minimally invasive establishment of murine orthotopic bladder xenografts. JoVE: e51123, 2014.

11 Teitz T, Stanke JJ, Federico S, Bradley CL, Brennan R, Zhang J, Johnson MD, Sedlacik J, Inoue M, Zhang ZM, Frase S, Rehg JE, Hillenbrand CM, Finkelstein D, Calabrese C, Dyer MA and Lahti JM: Preclinical Models for Neuroblastoma: Establishing a Baseline for Treatment. PLoS ONE *6*: e19133, 2011.

12 Cheng H, Clarkson PW, Gao D, Pacheco M, Wang Y and Nielsen TO: Therapeutic Antibodies Targeting CSF1 Impede Macrophage Recruitment in a Xenograft Model of Tenosynovial Giant Cell Tumor. Sarcoma *2010*: 174528-174527, 2010.

13 Cutz J-C, Guan J, Bayani J, Yoshimoto M, Xue H, Sutcliffe M, English J, Flint J, LeRiche J, Yee J, Squire JA, Gout PW, Lam S and Wang Y-Z: Establishment in severe combined immunodeficiency mice of subrenal capsule xenografts and transplantable tumor lines from a variety of primary human lung cancers: potential models for studying tumor progression-related changes. Clin Cancer Res *12*: 4043-4054, 2006.

14 Mendoza-Naranjo A, El-Naggar A, Wai DH, Mistry P, Lazic N, Ayala FRR, da Cunha IW, Rodriguez-Viciana P, Cheng H, Tavares Guerreiro Fregnani JH, Reynolds P, Arceci RJ, Nicholson A, Triche TJ, Soares FA, Flanagan AM, Wang YZ, Strauss SJ and Sorensen PH: ERBB4 confers metastatic capacity in Ewing sarcoma. EMBO Mol Med *5*: 1019-1034, 2013.

15 Dickman PS, Liotta LA and Triche TJ: Ewing's sarcoma. Characterization in established cultures and evidence of its histogenesis. Lab Invest *47*: 375-382, 1982.

16 Llombart-Bosch A, Carda C, Peydró-Olaya A, Noguera R, Perez-Bacete M, Pellin A and Boix J: Soft tissue Ewing's sarcoma. Characterization in established cultures and xenografts with evidence of a neuroectodermic phenotype. Cancer *66*: 2589-2601, 1990.

17 May WA, Grigoryan RS, Keshelava N, Cabral DJ, Christensen LL, Jenabi J, Ji L, Triche TJ, Lawlor ER and Reynolds CP: Characterization and Drug Resistance Patterns of Ewing's Sarcoma Family Tumor Cell Lines. PLoS ONE *8*: e80060, 2013.
18 Ikeda AK, Judelson DR, Federman N, Glaser KB, Landaw EM, Denny CT and Sakamoto KM: ABT-869 inhibits the proliferation of Ewing Sarcoma cells and suppresses platelet-derived growth factor receptor beta and c-KIT signaling pathways. Mol Cancer Ther *9*: 653-660, 2010.
19 Citrin D and Camphausen K: Optical imaging of mice in oncologic research. Expert Rev Anticancer Ther *4*: 857-864, 2004.
20 Braekeveldt N, Wigerup C, Gisselsson D, Mohlin S, Merselius M, Beckman S, Jonson T, Borjesson A, Backman T, Tadeo I, Berbegall AP, Øra I, Navarro S, Noguera R, Påhlman S and Bexell D: Neuroblastoma patient-derived orthotopic xenografts retain metastatic patterns and geno- and phenotypes of patient tumours. Int J Cancer *136*: E252-E261, 2015.
21 Ngiow SF, Loi S, Thomas D and Smyth MJ: Mouse Models of Tumor Immunotherapy. *In*: Tumor Immunology. Elsevier, pp. 1-24, 2016.
22 Izumchenko E, Meir J, Bedi A, Wysocki PT, Hoque MO and Sidransky D: Patient-derived xenografts as tools in pharmaceutical development. Clin Pharmacol Ther *99*: 612-621, 2016.
23 Li J, Ye C and Mansmann UR: Comparing Patient-Derived Xenograft and Computational Response Prediction for Targeted Therapy in Patients of Early-Stage Large Cell Lung Cancer. Clin Cancer Res *22*: 2167-2176, 2016.

Received June 26, 2017
Revised July 14, 2017
Accepted July 17, 2017